J. Neural Eng. **4** (2007) 264–275 doi:10.1088/1741-2560/4/3/012

Decoding two-dimensional movement trajectories using electrocorticographic signals in humans

G Schalk[1,2], J Kubánek[1,3], K J Miller[4,5], N R Anderson[6], E C Leuthardt[7,8], J G Ojemann[7], D Limbrick[8], D Moran[6], L A Gerhardt[2] and J R Wolpaw[1]

[1] BCI R&D Progr, Wadsworth Ctr, NYS Department of Health, Albany, NY, USA
[2] Elec, Comp, and Syst Eng Department, Renss Polyt Inst, Troy, NY, USA
[3] Department of Cybern, Czech Tech University, Prague, Czech Republic
[4] Department of Physics, University of Washington, Seattle, WA, USA
[5] Department of Medicine, University of Washington, Seattle, WA, USA
[6] Department of Biomed Eng, Washington University, St. Louis, MO, USA
[7] Department of Neurosurgery, University of Wash School of Med, Seattle, WA, USA
[8] Department of Neurol Surg, Barnes-Jewish Hospital, St. Louis, MO, USA

E-mail: schalk@wadsworth.org

Received 27 September 2006
Accepted for publication 30 May 2007
Published 22 June 2007
Online at stacks.iop.org/JNE/4/264

Abstract
Signals from the brain could provide a non-muscular communication and control system, a brain–computer interface (BCI), for people who are severely paralyzed. A common BCI research strategy begins by decoding kinematic parameters from brain signals recorded during actual arm movement. It has been assumed that these parameters can be derived accurately only from signals recorded by intracortical microelectrodes, but the long-term stability of such electrodes is uncertain. The present study disproves this widespread assumption by showing in humans that kinematic parameters can also be decoded from signals recorded by subdural electrodes on the cortical surface (ECoG) with an accuracy comparable to that achieved in monkey studies using intracortical microelectrodes. A new ECoG feature labeled the local motor potential (LMP) provided the most information about movement. Furthermore, features displayed cosine tuning that has previously been described only for signals recorded within the brain. These results suggest that ECoG could be a more stable and less invasive alternative to intracortical electrodes for BCI systems, and could also prove useful in studies of motor function.

M This article features online multimedia enhancements

(Some figures in this article are in colour only in the electronic version)

1. Introduction

Brain–computer interfaces (BCIs) use brain signals to communicate a user's intent [1]. Because these systems do not depend on peripheral nerves and muscles, they can be used by people with severe motor disabilities. Practical applications of BCI technology are currently impeded by the limitations and requirements of non-invasive and invasive methods.

Non-invasive BCIs use electroencephalographic activity (EEG) recorded from the scalp [1]. While non-invasive BCIs can support multidimensional control [2], their use requires extensive user training. Invasive BCIs use activity from multiple neurons recorded within the brain [3–6]. Signals recorded within cortex have higher fidelity and might support BCI systems that require less training than EEG-based systems. However, clinical implementations are impeded

 © 2007 IOP Publishing Ltd Printed in the UK

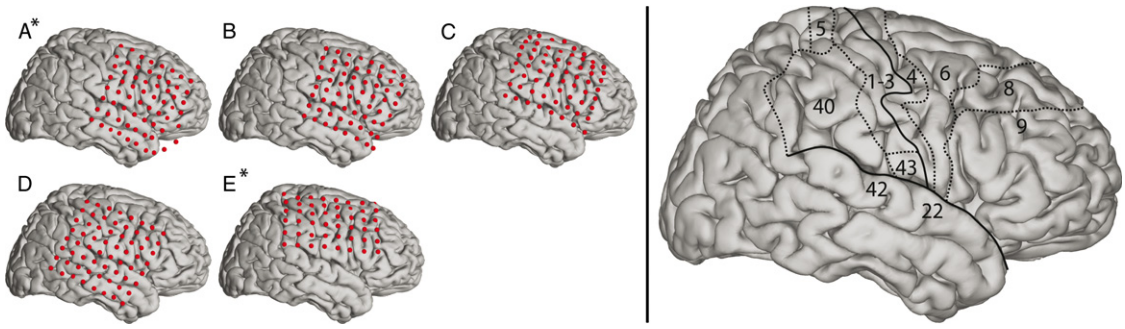

Figure 1. Electrode locations in the five subjects. The electrodes were projected on the right hemisphere for subjects A and E (see asterisks). The brain template on the bottom right highlights the location of the central sulcus and Sylvian fissure, and also outlines relevant Brodmann areas.

Table 1. Clinical profiles. All subjects were literate and functionally independent. Subject A had a prior left anterior temporal lobectomy. Subject B had no traumatic or structural lesion. Subject C had a right anterior frontal traumatic injury. Subject D had a right posterior temporal arteriovenous malformation embolized 20 years earlier. Subject E had a left frontal dysembryoplastic neuroepithelial tumor.

Subject	Age	Sex	Hand	Cognitive capacity	Grid location	Seizure focus
A	23	M	R	Normal (IQ 88)	Left frontal temporal	Left temporal
B	24	F	R	Normal (IQ 97)	Right frontal temporal	Right orbitofrontal and temporal
C	38	M	R	Borderline (IQ 70)	Right frontal	Right frontal
D	48	M	R	Normal (IQ 82; Right sup quadr visual deficit)	Right temporal	Right temporal occipital focus
E	18	F	R	Normal (IQ 86)	Left frontal	Left frontal

mainly by the risks of surgical implantation and by the substantial problems in achieving and maintaining stable long-term recordings [7, 8]. While a few recent studies have begun to apply non-invasive and invasive BCI technologies to the needs of severely disabled individuals [9, 10], these issues remain crucial obstacles that currently prohibit widespread clinical use in humans.

In the current absence of techniques to extract high-fidelity signals from EEG and of methods to record activity from within the brain safely and over long periods, the use of electrocorticographic activity (ECoG) recorded from the cortical surface could be a powerful and practical alternative. ECoG has higher spatial resolution than EEG (i.e., tenths of millimeters versus centimeters), broader bandwidth (i.e., 0–500 Hz [11] versus 0–40 Hz), higher amplitude (i.e., 50–100 μV maximum versus 10–20 μV), and far less vulnerability to artifacts such as EMG [12]. At the same time, because ECoG does not require electrodes that penetrate cortex, it is likely to have greater long-term stability [13–17] and to produce less tissue damage.

We previously showed that ECoG signals associated with imagery of arbitrary tasks can provide one-dimensional BCI control with little training [18]. It is possible that using more intuitive tasks (such as imagined hand movements) might more efficiently extend this control to multiple dimensions. However, most studies that decoded hand movements from brain signals have been in monkeys [19–21]. Only limited relevant information is available in humans [18, 22, 23].

In this study, we set out to determine if it is possible to faithfully decode in real time kinematic parameters from ECoG signals recorded in humans. We studied five subjects who were asked to use a joystick to move a cursor so as to track a target that moved on a computer screen. The principal results show that ECoG signals can be used to accurately decode two-dimensional joystick kinematics in humans. They also show that these results are within the range of those achieved in studies using intracortical microelectrode recordings in monkeys that also aimed to decode two-dimensional kinematic parameters. Furthermore, they indicate that a new brain signal component, which we label the local motor potential (LMP), holds substantial information about movement direction. Finally, ECoG features can also exhibit the same kind of cosine tuning previously detected only with intracortical microelectrodes in monkeys [21, 24–32]. These results provide strong evidence that ECoG could be used to provide accurate multidimensional BCI control, and also suggest that ECoG is a potentially powerful tool for the study of brain function.

2. Methods

2.1. Subjects

The subjects in this study were five patients with intractable epilepsy who underwent temporary placement of subdural electrode arrays to localize seizure foci prior to surgical resection. They included three men (subjects A, C and D) and two women (subjects B and E). (See table 1 for additional information.) All gave informed consent. The study was approved by the Institutional Review Board of the University of Washington School of Medicine. Each subject had a 48- or 64-electrode grid placed over the fronto-parietal-temporal region including parts of sensorimotor cortex (see figure 1 for details). These grids consisted of flat electrodes with a

diameter of 4 mm (2.3 mm exposed) and an inter-electrode distance of 1 cm, and were implanted for about 1 week. Grid placements and duration of ECoG monitoring were based solely on the requirements of the clinical evaluation, without any consideration of this study. Following placement of the subdural grid, each subject had postoperative anterior–posterior and lateral radiographs to verify grid location.

2.2. Experimental paradigm

During the study, each subject was in a semi-recumbent position in a hospital bed about 1 m from a video screen. He/she used a joystick with the hand contralateral to the implanted electrode array to move a white cursor in two dimensions to track a green target. The target moved counter-clockwise in a circle that was positioned in the center of a computer screen. The target encouraged the subjects, who were often impaired by post-operative recovery, to engage in continuous movements. Substantial variability in the subjects' tracking trajectories allowed us to make additional inferences about different aspects of the movement (see section 4 for details). The diameter of the circle was 61% (one subject) or 85% (all other four subjects) of the screen's height. One full revolution of the target took 6.3 s for all subjects. (At the same movement speed, a typical center-out task (i.e., moving a cursor from the center of the screen to the periphery of the screen) would have had a movement duration of less than 1.2 s.) To allow for offline analyses, the position of the cursor and the target were stored along with the digitized ECoG signals. Joystick position was mapped to cursor velocity and the joystick produced significant force feedback to the subject so that this task approached the isometric force tasks used in [33–35]. Subjects were asked to use shoulder and proximal arm movements rather than wrist movements. They were also asked to maintain a constant posture, but neither body, head, nor hand were restrained in any way.

2.3. Data collection

In all experiments, we recorded ECoG from the electrode grid using the general-purpose BCI system BCI2000 [36] connected to a Neuroscan Synamps2 system. Simultaneous clinical monitoring was achieved using a connector that split the cables coming from the subject into one set that was connected to the clinical monitoring system and another set that was connected to the BCI2000/Neuroscan system. Thus, at no time was clinical care or clinical data collection compromised. All electrodes were referenced to an inactive electrode. The signals were amplified, bandpass filtered between 0.15 and 200 Hz, digitized at 1000 Hz, and stored in BCI2000. The amount of data obtained varied from subject to subject, and depended on the subject's physical state and availability. The duration of the datasets averaged 443 s (range 130–830 s). Each dataset was visually inspected and all channels that did not clearly contain ECoG activity (e.g., such as channels that contained flat signals or noise due to broken connections) were removed prior to analysis, which left 48–64 channels for our analyses.

2.4. 3D cortical mapping

We used lateral skull radiographs to identify the stereotactic coordinates of each grid electrode with software [37] that duplicated the manual procedure described in [38]. We defined cortical areas using Talairach's Co-Planar Stereotaxic Atlas of the Human Brain [39] and a Talairach transformation (http://ric.uthscsa.edu/projects/talairachdaemon.html). We obtained a template 3D cortical brain model (subject-specific brain models were not available) from source code provided on the AFNI SUMA website (http://afni.nimh.nih.gov/afni/suma). Finally, we projected each subject's electrode locations on this 3D brain model and generated activation maps using a custom Matlab program.

2.5. Feature extraction and selection

We first re-referenced the signal from each electrode using a common average reference (CAR) montage. To do this, we obtained the CAR-filtered signal s'_h at channel h using $s'_h = s_h - \frac{1}{H}\sum_{q=1}^{H} s_q$. H was the total number of channels and s_h was the original signal sample at a particular time.

For each 333 ms time period (overlapping by 166 ms), we then converted the time-series ECoG data into the frequency domain with an autoregressive model [40] of order 50. Using this model, we calculated spectral amplitudes between 0 and 200 Hz in 1 Hz bins. We averaged these spectral amplitudes in particular frequency ranges (8–12 Hz, 18–24 Hz, 35–42 Hz, 42–70 Hz, 70–100 Hz, 100–140 Hz, 140–190 Hz) in the mu, beta and gamma frequency bands, similar to those used in [21]. In addition, visual inspection identified specific channels in which ECoG voltage level appeared to correlate with kinematic parameters. It thus seemed that these locations were amplitude-modulated in the time-domain (i.e., exhibiting the local motor potential (LMP)) rather than in a low band in the frequency-domain.

Figure 2 shows an example ECoG time course for subject C (A), the spatial distribution of channels that exhibit the LMP (B), and the magnified time course of channel 35, as well as the X position of the cursor and moving target (C). The correlation of the ECoG time course with the movement parameters is evident and clearly focused on select channels over hand sensorimotor cortex. The magnification shown in (C) demonstrates an example of good correlation between ECoG time course (black trace) with the X position of the cursor (thick dark green trace). It also illustrates an example of modest tracking performance indicated by the poor concurrence between the X position of the cursor (thick dark green trace) and the X position of the moving target (thin light green trace) between 45 and 60 s.

To account for the possibility of movement-related LMP modulation, we added to the frequency-based features listed above the 333 ms running average of the raw unrectified signal. This yielded eight features per channel, i.e., a total maximum of $8 \times 64 = 512$ features. Finally, we applied a running average filter (boxcar window, length was 9 samples (9×166 ms $= 1494$ ms)) to each of these features.

To reduce this large number of features, we employed the correlation-based feature selector (CFS) that is implemented in

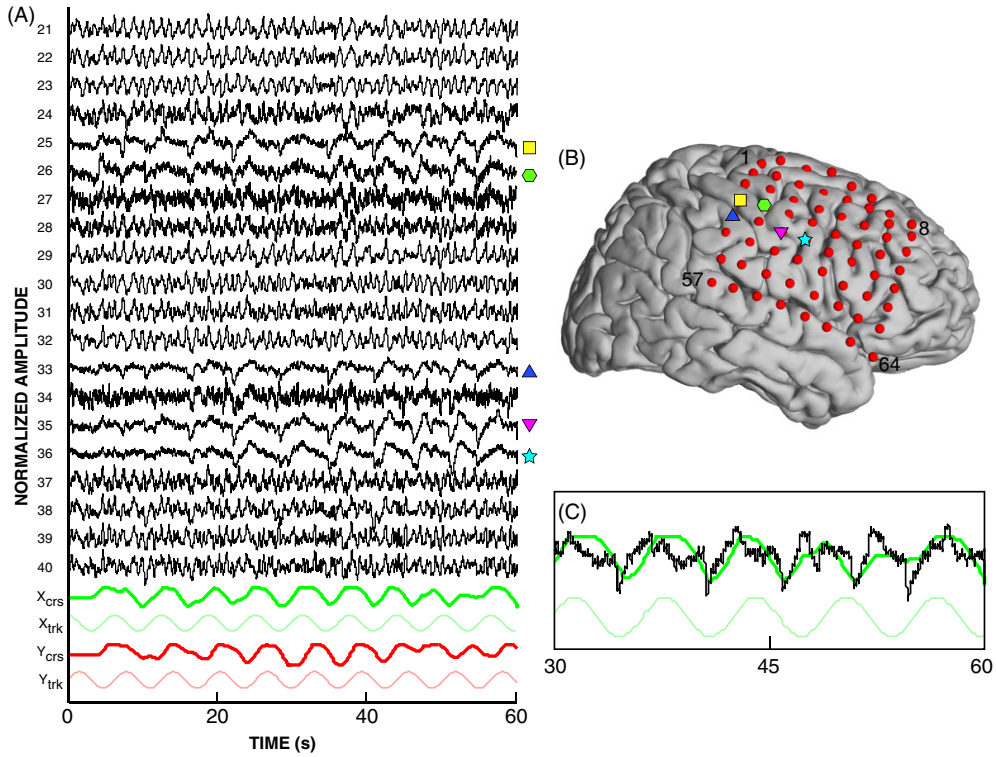

Figure 2. Example ECoG time course for subject C. (A) Time course of ECoG signals for channels 21–40 and for the X position of the cursor (X_{crs}), the X position of the tracking target (X_{trk}), as well as the Y position of the cursor (Y_{crs}) and target (Y_{trk}). Channels that exhibit a time course that is correlated with the movement parameters X_{crs} or Y_{crs} (i.e., a time course exhibiting the LMP) are indicated with symbols. (B) Electrode locations including channel numbers. Symbols indicate the locations of channels that show the LMP. (C) Magnification of ECoG time course of channel 35 from 30 to 60 s, as well as the X position of the cursor (thick dark green trace) and the X position of the moving target (thin light green trace).

the Java-based Weka package [41], which ranks feature subsets rather than individual features. (It thereby takes into account not only the correlation of any one particular feature with the values to be decoded, but also the cross-correlation between features.) The use of this procedure reduced the number of features to 5–20 (10 on average) for the different datasets.

2.6. Classification

Using the ECoG features selected by the CFS procedure, we then derived one linear model for each of the four kinematic parameters of the subject's cursor (i.e., horizontal position, vertical position, horizontal velocity, vertical velocity). We used the ECoG features to decode each of the four kinematic parameters immediately following the period representing these features (i.e., causal prediction) so that the same procedure could be used in real time.

2.7. Evaluation

The performance of the linear models was evaluated using 5-fold cross-validation, i.e., each dataset was divided into five parts, the linear models were determined from 4/5th of the dataset (training set) and tested (i.e., the coefficients of the linear model derived using the regression were applied) on the remaining 1/5th (test set). This procedure was then repeated five times—each time, a different 1/5th of the dataset was used as the test set. (The feature selection procedure was always applied to the training set only.)

We evaluated the performance of each of the five models by cross-correlating the decoded kinematic parameters with the actual values for position and velocity. This resulted in a correlation coefficient r for each dataset, cross-validation fold, and each of the four kinematic parameters.

2.8. Directional tuning

In additional analyses, we determined the relationship between each ECoG feature f and the direction (i.e., angle) of movement. To do this, we assigned, for each cross-validation fold of each dataset, the feature samples $\boldsymbol{f}$ to the corresponding movement direction, which we discretized in 20 equidistant bins from -180 to $+180^\circ$. Depending on the length of the dataset and the joystick movement patterns, each of these bins contained a variable amount of feature samples (19 on average). The 20 bins i and the distribution of feature samples $\boldsymbol{f}_i$ within each bin defined a *tuning curve* for each feature, location, cross-validation fold and subject. We then determined whether these observed tuning curves were a function of movement direction (i.e., they were *tuned*) or a cosine function of movement direction (i.e., they were *cosine tuned*), similar to the approach in [21]. This procedure is described in short below.

To determine whether a curve was tuned, we calculated the probability that each tuning curve differed from randomly generated tuning curves. To do this, we first calculated a tuning index measure SNR that related the variance of all feature values $\sigma^2(\boldsymbol{f})$ to the average variance of the feature values within each bin $\left(\frac{1}{20}\sum_{i=1}^{20}\sigma^2(\boldsymbol{f}_i)\right)$: $\mathrm{SNR} = \frac{\sigma^2(\boldsymbol{f})}{\frac{1}{20}\sum_{i=1}^{20}\sigma^2(\boldsymbol{f}_i)}$. Then, we shuffled all feature values such that they were assigned to randomly chosen bins, calculated the value of SNR, and repeated this procedure 200 times, which resulted in 200 measures of SNR. We modeled these measurements using a Gaussian distribution (i.e., we calculated the SNR mean and standard deviation)[1]. We finally determined the probability *pt* that the value of SNR for the observed tuning curve was generated by the Gaussian model distribution of randomly generated SNR values. A tuning curve was considered tuned if *pt* was smaller than 0.001.

For each tuning curve that was considered tuned, we also determined whether it was cosine tuned. To do this, we calculated the mean value $\overline{\boldsymbol{f}_i}$ of all features within each bin, which defined the average observed tuning curve. We then calculated the correlation coefficient *r* between this average tuning curve and a cosine function that was fit through to this curve. Similar to above, we then determined the probability *pct* that the observed tuning curve was generated by a distribution of randomly generated *r* values. A tuning curve was considered cosine tuned if *pct* was smaller than 0.001.

3. Results

To study the fidelity of the trajectory decoding and the characteristics of the associated brain signals, we determined the accuracy of decoded cursor position and velocity, compared it to published results using implanted microelectrodes, and established the anatomical location and ECoG features that held the most information. We also determined the anatomical location and ECoG features that were cosine tuned to movement direction. The results of these evaluations are described below.

3.1. Accurate decoding of kinematic parameters

Table 2 shows the principal results of this study, which are given in correlation coefficients calculated between actual and decoded kinematic parameters. The generally high correlation coefficients demonstrate that it is possible to infer accurate information about joystick kinematic parameters in real time using ECoG signals in humans (see figure 3 and the movie in the supplementary material at stacks.iop.org/JNE/4/264 for actual and decoded trajectories). Because the calculation of decoding parameters only involves the training dataset, but not the test dataset, similar results can be expected in online experiments.

Table 3 compares the results of the present study to those previously reported for decoding of two-dimensional movement parameters using intracortical implants in non-human primates. This table shows that the correlation of the actual with the decoded trajectories, and thus the fidelity of the decoding, reported in the present study, is within the range of those achieved before only using implanted microelectrodes.

Table 2. Decoding of kinematic parameters. Correlation coefficients (r) between the actual and decoded kinematic parameters (horizontal position of the cursor (X), vertical position (Y), horizontal velocity (V_x) and vertical velocity (V_y)) and the average across kinematic parameters (Avg r). Top group: correlation coefficients are given, for each parameter and dataset, for the worst and the best of the five cross-validation folds. Bottom group: median values of correlation between the actual and decoded kinematic parameters, calculated across all five cross-validation folds. These results demonstrate that good reconstruction of kinematic parameters (on data that were not used to train the algorithm) is possible using ECoG signals in humans.

Subject	X	Y	V_x	V_y	Avg r
A	0.49–0.61	0.20–0.49	0.18–0.48	0.39–0.66	
B	0.19–0.60	−0.13–0.72	0.03–0.73	0.18–0.52	
C	0.50–0.81	0.18–0.80	0.04–0.35	0.45–0.85	
D	0.40–0.64	0.28–0.78	0.30–0.72	0.58–0.68	
E	0.14–0.52	0.04–0.48	0.09–0.61	0.11–0.66	
A	0.58	0.38	0.42	0.59	0.49
B	0.42	0.55	0.59	0.32	0.47
C	0.71	0.51	0.10	0.67	0.50
D	0.57	0.68	0.58	0.66	0.62
E	0.37	0.22	0.32	0.49	0.35

3.2. Relative importance of anatomical areas and eCoG features

We also studied the relative importance of the different anatomical areas and ECoG features (i.e., the seven frequency-based features and the LMP) that were implicated in the decoding of cursor position and velocity. To do this, we analyzed the data as described before except that we first normalized the features with respect to their standard deviations[2]. This allowed the weights that were derived by the linear regression and associated with particular features and locations to be used as a measure of importance in decoding a certain kinematic parameter. We then used the CFS feature selection procedure and linear regression to produce weights for specific features at particular locations for the best four cross-validation folds in each subject, and for each of the four kinematic parameters. We finally removed the bias due to the number of electrodes by normalizing each set of weights by the sum of all weights.

To determine the relative importance of different anatomical areas, we then simply accumulated the weights for each location (so that one electrode could be assigned multiple weights from different folds and/or features) and plotted the results on a 3D model of the cortex. (Subjects A and E had electrode grids on the left hemisphere. We projected the electrode locations from these subjects to the

[1] We assessed the normality of these measurements using a Kolmogorov–Smirnoff test. This test determined that 90% of all distributions were considered Gaussian at the 0.05 level.

[2] We did not utilize this normalization before because we were interested in deriving results that could have been achieved in real time. We here calculated the standard deviation on the whole dataset, which cannot be performed in real time.

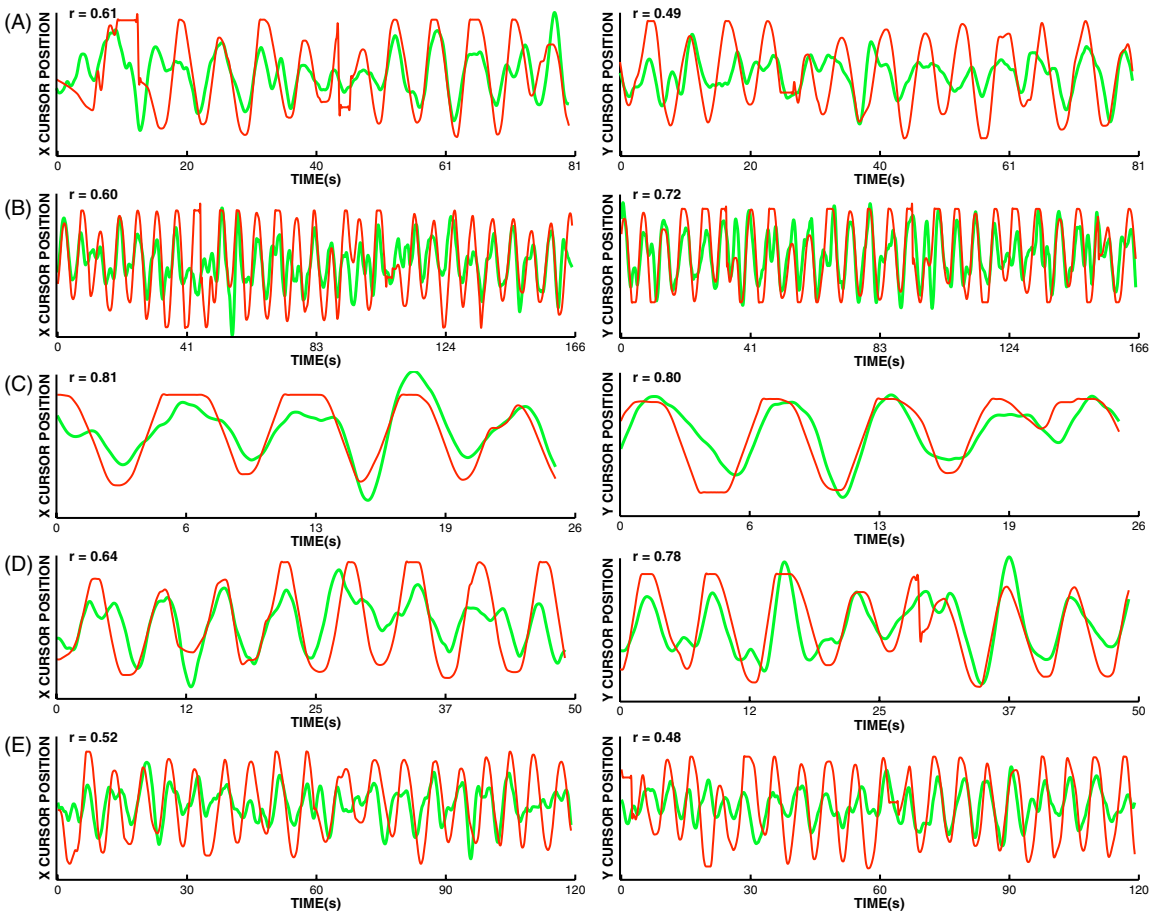

Figure 3. Actual and decoded movement trajectories. This figure shows examples for actual (thin red traces) and decoded (thick green traces) *X* and *Y* cursor position for all subjects (for the best cross-validation fold for each of *X* and *Y* cursor position), as well as the respective correlation coefficients *r*. The high correlation coefficients evidence the generally close concurrence between actual and decoded cursor positions.

Table 3. Comparison to intracortical studies. We compared the results of the present study to published results using two-dimensional tasks and microelectrode recording in monkeys. (We included only those reports that described methods that could have been achieved in real time.) Average correlation coefficients for published position and/or velocity values (Position *r* and Velocity *r*, respectively) across all subjects are shown. The correlation of the actual with the decoded trajectories, and thus the fidelity of the decoding, reported in the present study, is within the range of those achieved using implanted microelectrodes in monkeys.

Study and source	Position *r*	Velocity *r*
Schwartz and Moran (1999, p 2713)	–	0.77
Carmena *et al* (2003, figures 1(F) and 3(C))	0.33–0.63	0.27–0.73
Paninski *et al* (2004, table 1)	0.47	–
Lebedev *et al* (2005, table 2)	–	0.56
Averbeck *et al* (2005, est. from figures 8(A) and (B))	–	0.74
Present study (2006, table 2)	0.50	0.48

right hemisphere to facilitate interpretation.) These results are shown in figure 4, which shows the topographical distribution of weights (color coded with red corresponding to the highest weight) accumulated for all features and subjects. Table 4 reports these weights broken down by Brodmann's area and ECoG feature.

These weights are generally high for motor and pre-motor cortical areas (Brodmann's area 4 and 6, respectively), but also for additional areas such as dorsolateral prefrontal cortex (which has been implicated in other guided motor tasks [42]) and those that do not have obvious motor control relevance (such as the activation at the tip of the temporal pole). The high weights reported in table 4 for the LMP also indicate the important contribution of the LMP to our results.

We draw four conclusions from these analyses. First, the cortex offers opportunities to infer kinematic parameters over widespread areas of cortex, not only over classical sensorimotor areas. This notion is consistent with a recent review on this topic [43]. Second, sensory cortex had only a modest influence, which suggests that movement decoding

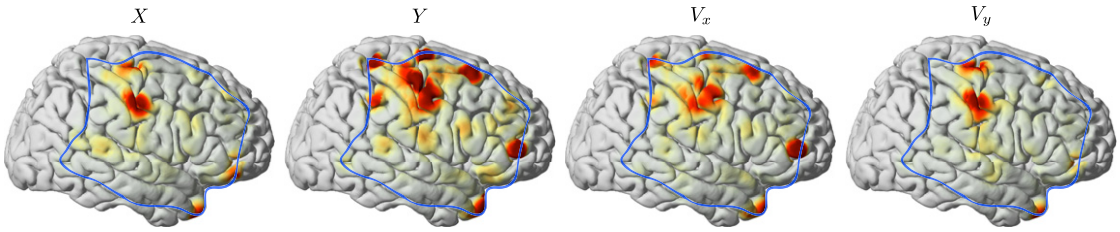

Figure 4. Anatomical areas holding information about movement parameters. Colors represent the weights accumulated for all features and subjects at the respective locations, and thus indicate the relative importance of these sites in decoding cursor position or velocity (transparent color and red correspond to zero and maximum weight, respectively). The weights are normalized for each movement parameter. The dominant focus over hand and proximal arm areas of motor cortex, indicated by the highest weights given to these areas, is evident. In addition, other locations are involved for which the anatomical relevance is not clear. The total area covered by the electrode grids in the five subjects is indicated by the blue outline.

Table 4. Relative importance of anatomical areas and ECoG features. The four tables contain weights assigned to signals in particular Brodmann's areas and ECoG features for cursor position and velocity. The two most important areas and features are given in bold. Motor and pre-motor cortices, as well as the LMP feature, held the highest weights, and thus the most information about kinematic parameters.

Horizontal cursor position

Area	8–12	18–24	35–42	42–70	70–100	100–140	**140–190**	**LMP**	SUM
1			0.10			0.06		0.40	0.55
2	0.02			0.06	0.38	0.63	0.99	0.19	2.28
3		0.14	0.21				0.60		0.94
4			0.07		0.18	0.51	1.44	0.99	**3.20**
6	0.20		0.18	0.33	0.17	0.46	0.10	1.05	**2.49**
7									
8	0.10							0.67	0.77
9		0.06		0.08	0.08	0.23	0.03	1.71	2.18
10	0.11							0.11	0.22
20	0.01								0.01
21	0.20	0.04					0.06	0.32	0.62
22	0.26		0.57	0.19				0.42	1.44
37	0.06								0.06
38	0.04						0.11	0.74	0.89
39									
40		0.19	0.19	0.15				0.66	1.19
42		0.04	0.05					0.29	0.38
43	0.13					0.07	0.02		0.22
44	0.11					0.04	0.13	0.39	0.67
45				0.08					0.08
46				0.05		0.06	0.02	0.52	0.66
47			0.18		0.21			0.79	1.18
SUM	1.23	0.45	1.55	0.94	1.01	2.06	**3.50**	**9.25**	

Vertical cursor position

Area	**8–12**	18–24	35–42	42–70	70–100	100–140	140–190	**LMP**	SUM
1				0.03				0.03	0.06
2	0.05	0.19	0.21	0.08	0.03	0.04		0.53	1.12
3	0.38			0.51	0.16	0.53	0.23	2.36	**4.16**
4	0.25		0.04		0.01		0.03	1.53	1.85
6	0.03	0.13	0.18	0.12				2.51	**2.97**
7		0.29	0.07						0.36
8			0.06		0.05		0.05	0.31	0.47
9	0.05	0.06				0.40	0.12	1.02	1.65
10	0.18								0.18
20									
21	0.08					0.17		0.09	0.35
22			0.14	0.05	0.10	0.08		0.31	0.69
37	0.06								0.06
38	0.18			0.09				1.02	1.29
39								0.01	0.01
40	0.05	0.01	0.05	0.18	0.13		0.04	0.57	1.03
42	0.10								0.10
43			0.18					0.16	0.34
44			0.13			0.05			0.19
45				0.07				0.03	0.11
46	0.04		0.07					1.30	1.40
47	0.11	0.08	0.10					1.34	1.63
SUM	**1.55**	0.75	1.22	1.14	0.48	1.27	0.47	**13.12**	

Horizontal cursor velocity

Area	8–12	18–24	**35–42**	42–70	70–100	100–140	140–190	**LMP**	SUM
1				0.05				0.17	0.23
2	0.20	0.05	0.25	0.02	0.13			1.10	1.76
3				0.08	0.07	0.34	0.34	1.07	1.89
4	0.15		0.24					2.38	**2.77**
6		0.33	0.14	0.21		0.03	0.09	2.19	**2.99**
7			0.28	0.03					0.31
8			0.08					0.40	0.48
9	0.07					0.31	0.04	0.83	1.25
10	0.14								0.14
11									
21					0.25	0.11	0.07	0.19	0.61
22				0.12			0.09	0.38	0.59
33									
37									
38	0.09		0.11				0.24	1.13	1.56
39				0.10					0.10
40	0.23			0.20	0.09			0.81	1.32
42							0.07		0.07
43		0.04				0.01		0.29	0.34
44			0.08						0.08
45				0.08			0.17		0.25
46		0.05	0.04				0.09	1.88	2.06
47								1.22	1.22
SUM	0.88	0.47	**1.22**	0.88	0.54	0.80	1.20	**14.02**	

Vertical cursor velocity

Area	8–12	18–24	35–42	42–70	70–100	100–140	**140–190**	**LMP**	SUM
1	0.05		0.12				0.06	0.31	0.54
2			0.08	0.08	0.18	0.54	1.42	0.08	2.38
3		0.04	0.30	0.12		0.06	1.17	0.01	1.70
4	0.06					0.07	1.12	1.33	**2.59**
6	0.21	0.05		0.42	0.07	0.25	0.19	1.91	**3.10**
7			0.03						0.03
8	0.04							0.56	0.60
9	0.04		0.10	0.06				1.06	1.25
10	0.07							0.13	0.19
11								0.78	0.78
21	0.08	0.07						0.47	0.62
22			0.13	0.06	0.05			0.51	0.75
33								0.11	0.11
37		0.06							0.06
38		0.11	0.09				0.06	0.67	0.93
39									
40		0.05	0.30	0.07				0.96	1.38
42						0.04		0.19	0.23
43	0.12						0.04	0.38	0.55
44								0.50	0.50
45	0.04	0.20						0.12	0.35
46	0.08	0.07				0.04		0.67	0.85
47		0.04	0.13		0.09			0.28	0.53
SUM	0.79	0.69	1.27	0.81	0.39	1.00	**4.06**	**11.01**	

is primarily related to the execution of movement and not to sensory feedback. Third, eye movements likely did not play a substantial role in movement decoding in our paradigm. Fourth, the evident anatomical relevance suggests that our signals are not an artifact but rather reflect physiological events related to movement control.

3.3. Directional tuning

The previous section described the importance of particular brain areas and ECoG features for the decoding of cursor position and velocity using a linear model. These analyses focused on decoding strategies that could be utilized in real time, which is important for potential brain–computer interfacing applications. Studies in the primate literature have also investigated the relationship of signal features with the movement direction (i.e., the angle of the movement). These studies (e.g., [24]) have shown that signal features (i.e., firing rates of particular neurons) that are derived from electrodes implanted within the brain can be *tuned*, i.e., are a function of movement direction, or even *cosine tuned*, i.e., are a cosine function of movement direction.

To study this possibility for our ECoG features, we investigated the effect of movement direction on feature amplitude using an approach similar to that employed in [21]. In short, we calculated the amplitudes of the eight features as a function of movement direction (i.e., the angle of the movement measured in -180 to $+180^{\circ}$). This produced one tuning curve for each subject, cross-validation fold, electrode location and feature. As described in section 2, we then derived the probabilities that the resulting tuning curves were tuned (pt) and cosine tuned (pct). We selected those tuning curves from the best four cross-validation folds that were tuned at $pt < 0.001$ and cosine tuned at $pct < 0.001$ and derived from each of them an index of cosine tuning ($ict = -\log_{10}(pct)$). As in the previous analysis, in which we used the CFS feature selector and linear regression, the present analysis derived measures (i.e., cosine tuning indices ict) for particular features at particular locations, cross-validation folds and subject. We then accumulated these cosine tuning measures across cross-validation folds and subjects and again projected the electrode locations for subjects A and E onto the right hemisphere.

The results of these analyses are shown in figure 5. This figure shows the cosine tuning indices, accumulated for all subjects and features (figure 5(A)) and for all subjects and each feature (figure 5(B)). These accumulated cosine tuning indices are color coded (see color bars). It is also shown in figure 5(C) three example LMP tuning curves for three subjects and for locations marked in the LMP in figure 5(B). The high values of the cosine tuning indices over primarily different motor cortical areas and for the LMP (the scale of the LMP in figure 5(B) is from 0 to 20) again validate the dominant role of these locations and this ECoG feature, respectively. Furthermore, the topographies of the tuning indices show substantial correlation for the different frequency features but are markedly different for the LMP. The tuning index topography for the LMP is more diffuse, but again peaks over hand area of motor cortex.

4. Discussion

In this study, we showed that ECoG signals can be used to accurately decode two-dimensional joystick trajectories in humans. We also characterized a new brain signal, the local motor potential (LMP), that holds substantial information about kinematic parameters. Furthermore, we demonstrated that ECoG features can exhibit the same kind of cosine tuning that has been previously described for neuronal firing rates and local field potentials (LFPs) recorded using intracortical microelectrodes [21, 44]. These results indicate that ECoG provides information that greatly exceeds in specificity that provided by EEG and is in important respects comparable to that provided by microelectrodes implanted in cortex. This study further implies that ECoG has characteristics that make it attractive not only for BCI research, but also for basic neuroscience investigations of brain function.

4.1. The local motor potential

The successful decoding of joystick movement achieved in this study depended in large part on the LMP component. Because no previous report has, to our knowledge, described the relationship of this new brain signal feature to kinematic parameters, we were concerned that it might be artifactual. Our results strongly indicate that this is not the case. First, the initial step in analysis was the application of a common average reference filter. This filter, which improved performance compared to when it was not applied, removes signals with low spatial frequencies such as those that would be expected for an artifact created by wire movement or some other external influence. Furthermore, analyses showed that the LMP was most often located over anatomically relevant areas, and that it could exhibit cosine tuning similar to that described for signals recorded by intracortical microelectrodes.

It is surprising that the LMP has apparently not been previously described in intracortical or scalp recordings. It is possible that the LMP cannot be detected on the scalp. Moreover, in our paradigm kinematic parameters changed relatively slowly (i.e., one full circle in 6.3 s = 0.16 Hz), whereas intracortical studies in monkeys often utilized higher speeds (i.e., around 1–2 Hz). In the latter cases, associated LMP components could have been masked by other activity. Alternatively, the LMP could be a continuous correlate to evoked LFP changes that have been described for other tasks, such as center-out [45] and reaching tasks [46]. Finally, it is possible that in previous studies the LMP component was filtered out at the amplification or post-processing stage. Indeed, when we re-analyzed data from our previous study [18] without applying a high-pass filter[3], we found that LMP amplitude in one particular location was modulated by the direction of joystick movement, and LMP amplitude in one immediately adjacent location was modulated by hand opening/closing and rest. These locations closely matched those that showed modulation of the spectral amplitude at

[3] In the previous study, we had analyzed signals from 0 to 200 Hz. However, we had subtracted the mean from each 280 ms window prior to analysis, which acted as a high-pass filter.

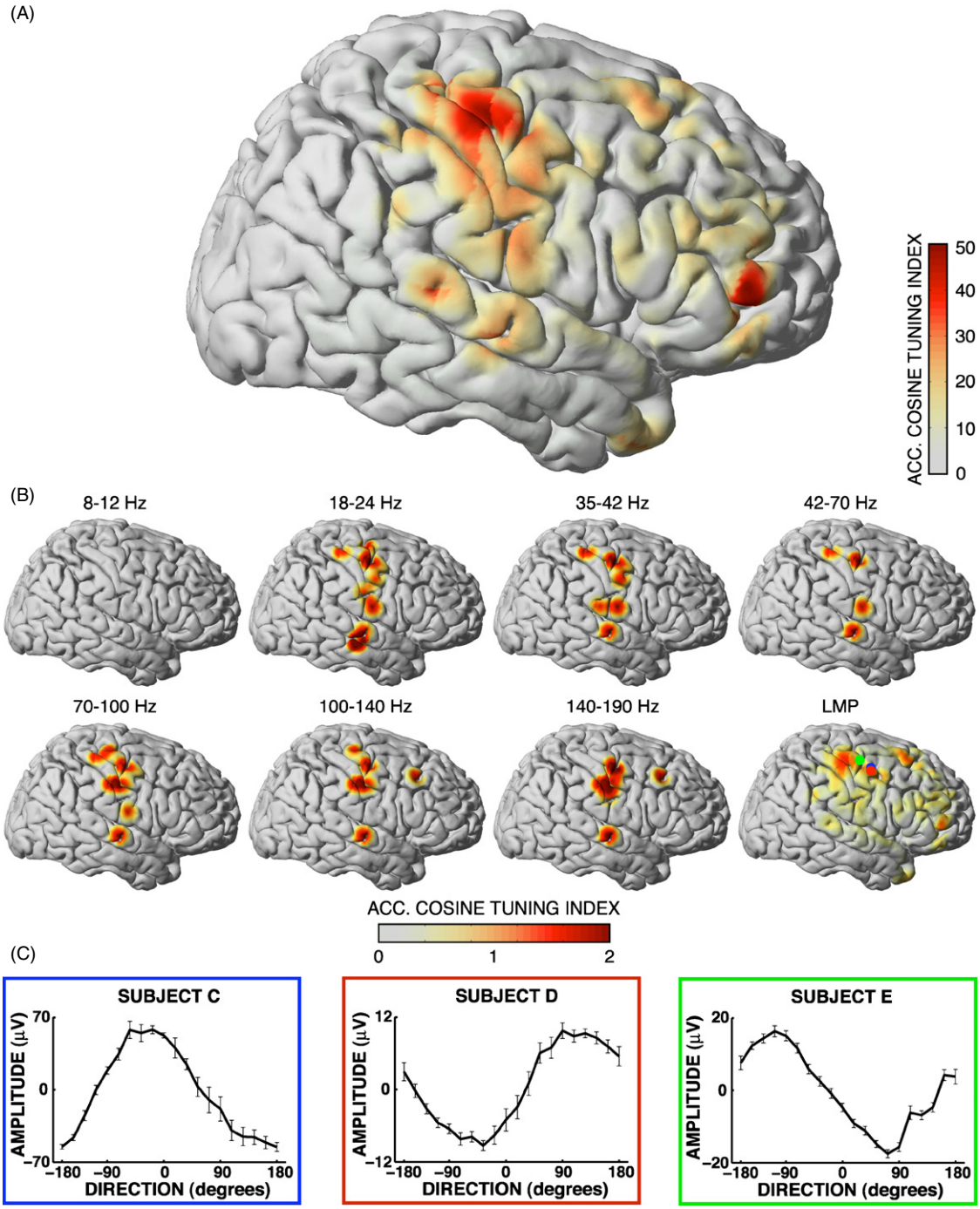

Figure 5. Cosine tuning. This figure shows the spatial distribution of the cosine tuning index, accumulated for all subjects and features (A), and for all subjects and each feature (B). The cosine tuning index is color coded (see color bars). The scale of the LMP figure in (B) is from 0 to 20. The tuning curves in (C) are calculated for the LMP at the locations marked in the LMP figure in (B).

18 Hz (i.e., a traditional frequency-based feature in the beta band). See the supplementary materials at stacks.iop.org/JNE/4/264 for details.

At this point, the physiological origin of the LMP component is a matter of speculation. It is possible that it reflects firing rate modulation of neurons located immediately underneath the electrode. In this case, the LMP may be related to the directionally-specific rate modulations observed in single-unit studies using center-out or tracking tasks [21, 47–54]. What complicates this interpretation is the fact that the tuning topographies for the LMP and frequency-based features are clearly different (see figure 5(B)), which suggests differing originating processes. Furthermore, it may be difficult to theoretically model the relationship between single-unit activity and ECoG activity as resulting ECoG activity could be dominated by the degree of synchronous activity of underlying cells rather than simply by the magnitude of cell activity. Hence, determination of the relationship

between these sources of brain signal activity will likely require simultaneous recordings of single-unit and ECoG activity (e.g., [55]), or at least of single-unit and local field potential activity (e.g., [20, 56, 57]).

4.2. Relevance for brain–computer interfaces

Together with results from previous studies in monkeys, the present results suggest that ECoG-based BCI use could be more intuitive, i.e., subjects could use movement-related imagery rather than imagery of arbitrary tasks for multidimensional BCI control. Thus, BCI training time might be reduced by using ECoG and movement-related imagery. At the same time, it is currently not clear what factors govern the need for BCI training time. It is possible that the physiological nature of the brain signal is important. In a typical mu- or beta-rhythm EEG-based BCI, brain signals associated with imagined limb movements are first identified. These signals are then used to provide one- or two-dimensional control. While the origins of these scalp-recorded rhythms are not entirely clear [58, 59], they are not believed to be strongly correlated with movement direction. Thus, their use for directional movement control might require considerable plasticity and user training. In contrast, BCI systems using implanted microelectrodes may require less user training. These systems typically utilize single-unit action potentials or local field potentials (LFPs) derived from neurons in motor cortex. Neurons are then identified that have firing rates/LPFs related to parameters of hand movements [24, 52, 53, 60–69]. They are then combined to produce multidimensional control signals. When monkeys are provided feedback based on brain signals rather than actual hand movements, they initially continue to move the hand but then learn to produce the same signals without the actual physical movements [4]. It is likely that the transformation of brain signals that typically encode movement direction into directional non-muscular commands demands less cortical reorganization and user training than the transformation of brain signals that do not normally encode direction, such as scalp-recorded mu and beta rhythms. Thus, the results of the present study, which show that kinematic parameters can be decoded from ECoG signals, suggest that the potential training-time advantage of implanted microelectrode recordings could also be achieved using ECoG.

For clinical applications of BCI technology, chronic implants of ECoG electrodes would be required. The literature suggests that subdural/epidural electrodes exhibit good long-term stability [13–17]. In addition, there are several theoretical reasons why ECoG electrodes will probably not be affected by the substantial stability problems associated with implanted microelectrodes. The area covered by each ECoG electrode is much larger, and thus its impedance much lower, than is the case for a microelectrode. Moreover, since ECoG electrodes do not penetrate cortex, the reactive responses of the brain typical with microelectrodes should be substantially reduced. Even if scar tissue were to form underneath the electrodes, the electrodes' low impedance should enable effective long term recordings. Furthermore, ECoG recordings require a dramatically lower bandwidth (i.e., 500 Hz sampling, and much less if only the LMP is extracted) than single-neuron recordings using microelectrodes (i.e., 10–50 kHz). These lower technical needs translate to substantially decreased processing and power requirements. Lower power requirements mean less heat dissipation and longer battery life. These substantial technical advantages will facilitate the design of electrode/telemitter systems that could be chronically implanted and would not require any percutaneous connection. This would greatly reduce the long-term risk of infection.

Our results did not depend on the circular trajectory of the target and were specific to the joystick movements. Tracking performance (i.e., how well the subjects tracked the target) was modest ($r = 0.56, r = 0.57, r = 0.50, r = 0.50$ calculated, for each of the kinematic parameters, between the cursor and the target, respectively) and not predictive of decoding performance ($p = 0.84, p = 0.88, p = 0.62, p = 0.91$ for the four kinematic parameters, respectively). This is inconsistent with the hypothesis that decoding performance is dependent on how well the subjects tracked the circular trajectory of the target. In summary, our results did not depend on the circular trajectory of the target and there was some degree of independence between the kinematic parameters. At the same time, the current paradigm was simply not designed to independently examine all four kinematic parameters. In consequence, future studies could expand on our initial results and utilize different movement patterns, directions and speeds, to determine how the results in humans using ECoG relate to the body of knowledge that has been established for signals recorded from intracortical microelectrodes.

4.3. Current experimental limitations

The present results strongly encourage further investigations using ECoG. At the same time, there will ultimately be limits to what can be achieved using the currently used patient population. Our study, like practically all human ECoG studies to date, relied on electrode grids implanted for clinical reasons. Thus, the grids often do not cover locations most appropriate for our purpose and, in addition, are different for each patient. Furthermore, the physical and cognitive condition and level of cooperation of each patient are impaired and/or variable. Finally, the patients' posture can be controlled for mostly only using instructions. This relatively uncontrolled experimental situation is in contrast to the typically rigorously controlled animal studies.

Despite these issues, the present results, in which we utilized all available data for each subject, compare favorably to results that have been achieved in highly controlled animal studies. At the same time, the present situation simply does not permit systematic studies using controlled experiments, which will ultimately limit the information that can be derived. We expect that the present results, and the results of the studies that will follow, will provide ample evidence of the utility of the ECoG platform to support FDA approval of subdural or epidural implants in humans for BCI purposes.

Acknowledgments

We thank Dr Elizabeth Winter Wolpaw for helpful comments on the manuscript. We also thank Drs Holmes and Miller for patient care and telemetry support. We further acknowledge the assistance of Drs Ashley, Dowling and Eisenman in the department of Neurological Surgery, Barnes Jewish Hospital, St Louis, in experiments leading up to the present study. Finally, we are grateful for the comments by the anonymous reviewers, which helped to greatly improve this paper. This work was supported in part by grants from NIH (EB006356 (GS), NS41272 (JO), HD30146 (JRW) and EB00856 (JRW)), the McDonnell Center for Higher Brain Function (JO) and the James S McDonnell Foundation (ECL and JRW).

References

[1] Wolpaw J R, Birbaumer N, McFarland D J, Pfurtscheller G and Vaughan T M 2002 Brain–computer interfaces for communication and control *Electroenceph. Clin. Neurophysiol.* **113** 767–91

[2] Wolpaw J R and McFarland D J 2004 Control of a two-dimensional movement signal by a noninvasive brain–computer interface in humans *Proc. Natl Acad. Sci. USA* **101** 17849–54

[3] Georgopoulos A P, Schwartz A B and Kettner R E 1986 Neuronal population coding of movement direction *Science* **233** 1416–9

[4] Taylor D M, Tillery S I and Schwartz A B 2002 Direct cortical control of 3D neuroprosthetic devices *Science* **296** 1829–32

[5] Serruya M D, Hatsopoulos N G, Paninski L, Fellows M R and Donoghue J P 2002 Instant neural control of a movement signal *Nature* **416** 141–2

[6] Lebedev M A, Carmena J M, O'Doherty J E, Zacksenhouse M, Henriquez C S, Principe J C and Nicolelis M A 2005 Cortical ensemble adaptation to represent velocity of an artificial actuator controlled by a brain–machine interface *J. Neurosci.* **25** 4681–93

[7] Shain W, Spataro L, Dilgen J, Haverstick K, Retterer S, Isaacson M, Satzman and Turner J N 2003 Controlling cellular reactive responses around neural prosthetic devices using peripheral and local intervention strategies *IEEE Trans. Neural Syst. Rehabil. Eng.* **11** 186–8

[8] Donoghue J P, Nurmikko A, Friehs G and Black M 2004 Development of neuromotor prostheses for humans *Suppl. Clin. Neurophysiol.* **57** 592–606

[9] Kübler A, Nijboer F, Mellinger J, Vaughan T M, Pawelzik H, Schalk G, McFarland D J, Birbaumer N and Wolpaw J R 2005 Patients with als can use sensorimotor rhythms to operate a brain–computer interface *Neurology* **64** 1775–7

[10] Hochberg L R, Serruya M D, Friehs G M, Mukand J A, Saleh M, Caplan A H, Branner A, Chen D, Penn R D and Donoghue J P 2006 Neuronal ensemble control of prosthetic devices by a human with tetraplegia *Nature* **442** 164–71

[11] Staba R J, Wilson C L, Bragin A, Fried I and Engel J 2002 Quantitative analysis of high-frequency oscillations (80–500 Hz) recorded in human epileptic hippocampus and entorhinal cortex *J. Neurophysiol.* **88** 1743–52

[12] Freeman W J, Holmes M D, Burke B C and Vanhatalo S 2003 Spatial spectra of scalp EEG and EMG from awake humans *Clin. Neurophysiol.* **114** 1053–68

[13] Loeb G E, Walker A E, Uematsu S and Konigsmark B W 1977 Histological reaction to various conductive and dielectric films chronically implanted in the subdural space *J. Biomed. Mater. Res.* **11** 195–210

[14] Bullara L A, Agnew W F, Yuen T G, Jacques S and Pudenz R H 1979 Evaluation of electrode array material for neural prostheses *Neurosurgery* **5** 681–6

[15] Yuen T G, Agnew W F and Bullara L A 1987 Tissue response to potential neuroprosthetic materials implanted subdurally *Biomaterials* **8** 138–41

[16] Pilcher W H and Rusyniak W G 1993 Complications of epilepsy surgery *Neurosurg. Clin. N. Am.* **4** 311–25

[17] Margalit E *et al* 2003 Visual and electrical evoked response recorded from subdural electrodes implanted above the visual cortex in normal dogs under two methods of anesthesia *J. Neurosci. Methods* **123** 129–37

[18] Leuthardt E C, Schalk G, Wolpaw J R, Ojemann J G and Moran D W 2004 A brain–computer interface using electrocorticographic signals in humans *J. Neural. Eng.* **1** 63–71

[19] Mehring C, Rickert J, Vaadia E, Cardosa de Oliveira S, Aertsen A and Rotter S 2003 Inference of hand movements from local field potentials in monkey motor cortex *Nat. Neurosci.* **6** 1253–4

[20] Andersen R A, Musallam S and Pesaran B 2004 Selecting the signals for a brain–machine interface *Curr. Opin. Neurobiol.* **14** 720–6

[21] Rickert J, Oliveira S C, Vaadia E, Aertsen A, Rotter S and Mehring C 2005 Encoding of movement direction in different frequency ranges of motor cortical local field potentials *J. Neurosci.* **25** 8815–24

[22] Toro C, Cox C, Friehs G, Ojakangas C, Maxwell R, Gates J R, Gumnit R J and Ebner T J 1994 8–12 Hz rhythmic oscillations in human motor cortex during two-dimensional arm movements: evidence for representation of kinematic parameters *Electroencephalogr. Clin. Neurophysiol.* **93** 390–403

[23] Georgopoulos A P, Langheim F J, Leuthold A C and Merkle A N 2005 Magnetoencephalographic signals predict movement trajectory in space *Exp. Brain Res.* **167** 132–5

[24] Georgopoulos A P and Massey J T 1988 Cognitive spatial-motor processes: 2. Information transmitted by the direction of two-dimensional arm movements and by neuronal populations in primate motor cortex and area 5 *Exp. Brain Res.* **69** 315–26

[25] Salinas E and Abbott L F 1994 Vector reconstruction from firing rates *J. Comput. Neurosci.* **1** 89–107

[26] Turner R S, Owens J W Jr and Anderson M E 1995 Directional variation of spatial and temporal characteristics of limb movements made by monkeys in a two-dimensional work space *J. Neurophysiol.* **74** 684–97

[27] Kettner R E, Marcario J K and Clark-Phelps M C 1996 Control of remembered reaching sequences in monkey: I. Activity during movement in motor and premotor cortex *Exp. Brain Res.* **112** 335–46

[28] Amirikian B and Georgopoulos A P 2000 Directional tuning profiles of motor cortical cells *Neurosci. Res.* **36** 73–9

[29] Baraduc P and Guigon E 2002 Population computation of vectorial transformations *Neural. Comput.* **14** 845–71

[30] Todorov E 2002 Cosine tuning minimizes motor errors *Neural. Comput.* **14** 1233–60

[31] Shoham S, Paninski L M, Fellows M R, Hatsopoulos N G, Normann R A and Donoghue J P 2005 Statistical encoding model for a primary motor cortical brain–machine interface *IEEE Trans. Biomed. Eng.* **52** 1312–22

[32] Nozaki D, Nakazawa K and Akai M 2005 Muscle activity determined by cosine tuning with a nontrivial preferred direction during isometric force exertion by lower limb *J. Neurophysiol.* **93** 2614–24

[33] Kalaska J F and Hyde M L 1985 Area 4 and area 5: differences between the load direction-dependent discharge variability of cells during active postural fixation *Exp. Brain Res.* **59** 197–202

[34] Taira M, Boline J, Smyrnis N, Georgopoulos A P and Ashe J 1996 On the relations between single cell activity in the motor cortex and the direction and magnitude of three-dimensional static isometric force *Exp. Brain Res.* **109** 367–76
[35] Sergio L E, Hamel-Pâquet C and Kalaska J F 2005 Motor cortex neural correlates of output kinematics and kinetics during isometric-force and arm-reaching tasks *J. Neurophysiol.* **94** 2353–78
[36] Schalk G, McFarland D J, Hinterberger T, Birbaumer N and Wolpaw J R 2004 BCI2000: a general-purpose brain–computer interface (BCI) system *IEEE Trans. Biomed. Eng.* **51** 1034–43
[37] Miller K J, Makeig S, Hebb A O, Rao R P, Dennijs M and Ojemann J G 2007 Cortical electrode localization from x-rays and simple mapping for electrocorticographic research: the 'location on cortex' (LOC) package for MATLAB *J. Neurosci. Methods* **162** 303–8
[38] Fox P T, Perlmutter J S and Raichle M E 1985 A stereotactic method of anatomical localization for positron emission tomography *J. Comput. Assist. Tomogr.* **9** 141–53
[39] Talairach J and Tournoux P 1988 *Co-Planar Sterotaxic Atlas of the Human Brain* (New York: Thieme Medical Publishers)
[40] Lawrence Marple S 1987 *Digital Spectral Analysis: With Applications* (Englewood Cliffs, NJ: Prentice-Hall)
[41] Witten I H and Frank Eibe 2005 *Data Mining: Practical Machine Learning Tools and Techniques* 2nd edn (San Francisco, CA: Morgan Kaufmann)
[42] Vaillancourt D E, Thulborn K R and Corcos D M 2003 Neural basis for the processes that underlie visually guided and internally guided force control in humans *J. Neurophysiol.* **90** 3330–40
[43] Davidson P R and Wolpert D M 2005 Widespread access to predictive models in the motor system: a short review *J. Neural. Eng.* **2** S313–9
[44] Heldman D A, Wang W, Chan S S and Moran D W 2006 Local field potential spectral tuning in motor cortex during reaching *IEEE Trans. Neural. Syst. Rehabil. Eng.* **14** 180–3
[45] Donchin O, Gribova A, Steinberg O, Bergman H, Cardoso de Oliveira S and Vaadia E 2001 Local field potentials related to bimanual movements in the primary and supplementary motor cortices *Exp. Brain Res.* **140** 46–55
[46] O'Leary J G and Hatsopoulos N G 2006 Early visuomotor representations revealed from evoked local field potentials in motor and premotor cortical areas *J. Neurophysiol.* **96** 1492–506
[47] Donoghue J P, Sanes J N, Hatsopoulos N G and Gaal G 1998 Neural discharge and local field potential oscillations in primate motor cortex during voluntary movements *J. Neurophysiol.* **79** 159–73
[48] Hatsopoulos N G, Ojakangas C L, Paninski L and Donoghue J P 1998 Information about movement direction obtained from synchronous activity of motor cortical neurons *Proc. Natl Acad. Sci. USA* **95** 15706–11
[49] Maynard E M, Hatsopoulos N G, Ojakangas C L, Acuna B D, Sanes J N, Normann R A and Donoghue J P 1999 Neuronal interactions improve cortical population coding of movement direction *J. Neurosci.* **19** 8083–93
[50] Donchin O, Gribova A, Steinberg O, Mitz A R, Bergman H and Vaadia E 2002 Single-unit activity related to bimanual arm movements in the primary and supplementary motor cortices *J. Neurophysiol.* **88** 3498–517
[51] Steinberg O, Donchin O, Gribova A, Cardosa de Oliveira S, Bergman H and Vaadia E 2002 Neuronal populations in primary motor cortex encode bimanual arm movements *Eur. J. Neurosci.* **15** 1371–80
[52] Rokni U, Steinberg O, Vaadia E and Sompolinsky H 2003 Cortical representation of bimanual movements *J. Neurosci.* **23** 11577–86
[53] Paninski L, Fellows M R, Hatsopoulos N G and Donoghue J P 2004 Spatiotemporal tuning of motor cortical neurons for hand position and velocity *J. Neurophysiol.* **91** 515–32
[54] Hatsopoulos N, Joshi J and O'Leary J G 2004 Decoding continuous and discrete motor behaviors using motor and premotor cortical ensembles *J. Neurophysiol.* **92** 1165–74
[55] Jones M S, MacDonald K D, Choi B, Dudek F E and Barth D S 2000 Intracellular correlates of fast (200 Hz) electrical oscillations in rat somatosensory cortex *J. Neurophysiol.* **84** 1505–18
[56] Pesaran B, Pezaris J S, Sahani M, Mitra P P and Andersen R A 2002 Temporal structure in neuronal activity during working memory in macaque parietal cortex *Nat. Neurosci.* **5** 805–11
[57] Jacobs Joshua, Kahana M J, Ekstrom A D and Fried I 2007 Brain oscillations control timing of single-neuron activity in humans *J. Neurosci.* **27** 3839–44
[58] Lopes da Silva F H 1991 Neural mechanisms underlying brain waves: from neural membranes to networks *Electroenceph. Clin. Neurophysiol.* **79** 81–93
[59] Niedermeyer E 2004 *The Normal EEG of the Waking Adult* 5th edn (Baltimore, MD: Williams and Wilkins) pp 167–92
[60] Schwartz A B and Moran D W 1999 Motor cortical activity during drawing movements: population representation during lemniscate tracing *J. Neurophysiol.* **82** 2705–18
[61] Moran D W and Schwartz A B 1999 Motor cortical activity during drawing movements: population representation during spiral tracing *J. Neurophysiol.* **82** 2693–704
[62] Moran D W and Schwartz A B 1999 Motor cortical representation of speed and direction during reaching *J. Neurophysiol.* **82** 2676–92
[63] Moran D W and Schwartz A B 2000 One motor cortex, two different views *Nat. Neurosci.* **3** 963–5
[64] Wessberg J, Stambaugh C R, Kralik J D, Beck P D, Laubach M, Chapin J K, Kim J, Biggs S J, Srinivasan M A and Nicolelis M A 2000 Real-time prediction of hand trajectory by ensembles of cortical neurons in primates *Nature* **408** 361–5
[65] Schwartz A B, Taylor D M and Tillery S I 2001 Extraction algorithms for cortical control of arm prosthetics *Curr. Opin. Neurobiol.* **11** 701–7
[66] Reina G A, Moran D W and Schwartz A B 2001 On the relationship between joint angular velocity and motor cortical discharge during reaching *J. Neurophysiol.* **85** 2576–89
[67] Merchant H, Battaglia-Mayer A and Georgopoulos A P 2004 Neural responses during interception of real and apparent circularly moving stimuli in motor cortex and area 7a *Cereb. Cortex* **14** 314–31
[68] Schwartz A B, Moran D W and Reina G A 2004 Differential representation of perception and action in the frontal cortex *Science* **303** 380–3
[69] Averbeck B B, Chafee M V, Crowe D A and Georgopoulos A P 2005 Parietal representation of hand velocity in a copy task *J. Neurophysiol.* **93** 508–18